Articles

Transition State Structure of *Salmonella typhimurium* Orotate Phosphoribosyltransferase†

Wen Tao,‡ Charles Grubmeyer,§ and John S. Blanchard*,‡

Department of Biochemistry, Albert Einstein College of Medicine, Bronx, New York 10461, and Department of Biochemistry, Temple University School of Medicine, Philadelphia, Pennsylvania 19140

Received August 14, 1995; Revised Manuscript Received October 23, 1995⊗

ABSTRACT: Orotate phosphoribosyltransferase (OPRTase) catalyzes the magnesium-dependent conversion of α-D-phosphoribosylpyrophosphate (PRPP) and orotate to orotidine 5′-monophosphate (OMP) and pyrophosphate. We have determined kinetic isotope effects on the reaction of OMP with pyrophosphate and with the pyrophosphate analog phosphonoacetic acid. In the latter case, full expression of the kinetic isotope effects allowed us to calculate the structure of the transition state for the pyrophosphorylytic reaction. The transition state resembles a classical oxocarbonium ion. Using the recently reported three-dimensional structures of the OPRTase−OMP (Scapin et al., 1994) and the OPRTase−PRPP complexes (Scapin et al., 1995a), we have modeled the calculated transition state structure into the active site of OPRTase. We propose a detailed chemical mechanism which is consistent with these results.

Orotate phosphoribosyltransferase (OPRTase; EC 2.2.4.10.) catalyzes the magnesium ion-dependent conversion of α-D-phosphoribosylpyrophosphate (PRPP) and orotate to orotidine 5′-monophosphate (OMP) and pyrophosphate. The *Salmonella typhimurium* enzyme, encoded by the *pyrE* gene, has been cloned, expressed (Bhatia et al., 1990), sequenced, and crystallized (Scapin et al., 1993) and functions as a homodimer of 213 amino acid residue monomers. The steady-state kinetic mechanism has been shown to be random sequential (Bhatia et al., 1990), and the reaction occurs with inversion of configuration at the anomeric position of PRPP (Chelsky & Parsons, 1975). Thirteen OPRTase sequences have been reported, and in addition to overall sequence homolgy, a short 12−13 residue sequence which contains adjacent carboxylate side chains of either glutamate or aspartate flanked by hydrophobic residues is highly conserved. This sequence also appears in the sequences of other PRTases and PRPP synthetase (Hove-Jensen et al., 1986), suggesting that it represents a PRPP binding motif (Hove-Jensen et al., 1986; Hersey & Taylor, 1986).

Phosphoribosyltransferases play key roles in both the *de novo* and salvage biosynthesis of purine, pyrimidine, and pyridine nucleotides (Musick, 1981). They are thus phylogenetically widely distributed. Ten members of the PRTase family are known, and genetic defects in the genes of several PRTases cause human pathologies. A defect in the human bifunctional OPRTase−OMP decarboxylase (UMP synthase) results in orotic aciduria and may also cause retardation (Suttle et al., 1989). Defects in the X-linked HPRT gene, encoding hypoxanthine−guanine phosphoribosyltransferase, causes Lesch−Nyhan syndrome, an inherited disorder characterized by gout, mental retardation, and self-mutilation (Stout & Caskey, 1989). Because of these key roles in nucleotide metabolism, and their ubiquitous distribution, the PRTases represent attractive targets for the rational design of antimicrobial, antiparasitic, and anticancer therapeutics.

One approach to such rational inhibitor design involves the determination of the structure of the transition state for the enzyme-catalyzed reaction (Schramm et al., 1994). These authors have developed methods for transition state structural analysis using the determination of kinetic isotope effects at multiple positions in the substrate molecule. Subsequent iterative modeling of potential transition states is performed until experimentally determined and calculated isotope effects are obtained which are in agreement. The method has shown excellent predictive and correlative success in the design of tight-binding inhibitors for trypanosomal nucleoside hydrolase (Horenstein et al., 1991; Horenstein & Schramm, 1993) and AMP deaminase (Merkler et al., 1993).

The chemical mechanism by which PRTases catalyze their reactions has been disputed for many years. Stereochemical results (Chelsky & Parsons, 1975) argue against mechanisms which invoke a covalent enzyme−phosphoribosyl intermediate used to rationalize early suggestions of a steady-state ping-pong kinetic mechanism (Victor et al., 1979). A direct S_N2-type displacement is possible given the inversion of configuration at the anomeric carbon position of PRPP; however, preliminary reports of large α-secondary tritium kinetic isotope effects exhibited by OPRTase, HGPRTase, and PRPP synthetase (Goitein et al., 1978) led to suggestions of two-step, S_N1-type mechanisms with oxocarbonium-like transition states or intermediates. Similar chemical mechanisms and transition state structures have been implicated in the hydrolytic reactions catalyzed by lysozyme (Kirby, 1987), AMP (Mentch et al., 1987), and inosine (Horenstein

† This work was supported by the National Institutes of Health (Grant GM 48623).

* Address correspondence to this author. Phone: (718) 430-3096. FAX: (718) 430-8565.

‡ Albert Einstein College of Medicine.

§ Temple University School of Medicine.

⊗ Abstract published in *Advance ACS Abstracts,* December 15, 1995.

0006-2960/96/0435-14$12.00/0

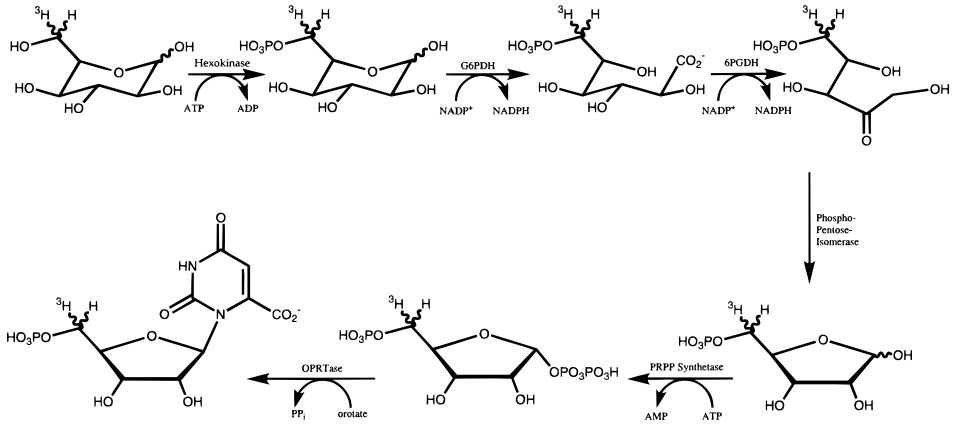

FIGURE 1: Enzymatic synthesis of OMP from labeled glucose, using [5′-^{3}H]OMP as an example. Abbreviations: PK, pyruvate kinase; G6PDH, glucose-6-phosphate dehydrogenase; GDH, glutamate dehydrogenase; 6PGDH, 6-phosphogluconate dehydrogenase; PRPP synthetase, 5-phosphoribosyl-1-pyrophosphate synthetase; PEP, phosphoenolpyruvate; αKG, α-ketoglutarate.

et al., 1991) nucleosidases and for purine nucleoside phosphorylase (Kline et al., 1993).

The determination of the 2.6 Å structure of the OPRTase−OMP complex (Scapin et al., 1994), and the more recently reported structure of the OPRTase−PRPP complex (Scapin et al., 1995), permits this powerful method of transition state structural analysis to be combined with detailed structural information concerning the interaction of the substrates and products with enzymic groups involved in binding and catalysis. Residues potentially involved in substrate deformation and transition state stabilization can be identified for more detailed mutagenic examination in such situations. We report here the determination of kinetic isotope effects on the *S. typhimurium* OPRTase-catalyzed pyrophosphorolysis of OMP to form orotate and PRPP. We have used the slow, alternative pyrophosphate analog phosphonoacetate (PA) to obtain values for the intrinsic kinetic isotope effects at various positions in the ribose ring of OMP. These results, and subsequent modeling of the transition state using the BEBOVIB program (Sims et al., 1977), argue persuasively for a transition state with *bona fide* oxocarbonium character and with substantial negative charge built up in the leaving orotate base. We propose a chemical mechanism which takes into account the residues present in the active site of OPRTase and the position of substrates and products on the enzyme surface.

EXPERIMENTAL PROCEDURES

Materials. [2-^{3}H]Glucose (21.5 Ci/mmol), [2-^{14}C]glucose (45 mCi/mmol), [5-^{3}H]glucose (15.7 Ci/mmol), [6-^{3}H]-glucose (36.2 Ci/mmol), and [6-^{14}C]glucose (51.8 mCi/mmol) were purchased from New England Nuclear. [1,3-$^{15}N_2$]-Orotate was purchased from Cambridge Isotope Laboratories. [2′-^{3}H]Ribose and 5-phosphoribosyl-1-pyrophosphate synthetase (EC 2.7.6.1) were the gifts of Dr. V. Schramm (Biochemistry, Albert Einstein College of Medicine). Hydrofluor scintillation fluid was purchased from National Diagnostics. Nucleogen DEAE columns were purchased from Rainin. All other enzymes and reagents were purchased from Sigma. Orotate phosphoribosyltransferase (EC 2.4.2.10) from *S. typhimurium* was purified as described previously (Bhatia et al., 1990).

Synthesis. [1′-^{3}H]OMP, [4′-^{3}H]OMP, [5′-^{3}H]OMP, [1′-^{14}C]OMP, and [5′-^{14}C]OMP were prepared enzymatically from [2-^{3}H]glucose, [5-^{3}H]glucose, [6-^{3}H]glucose, [2-^{14}C]-glucose, and [6-^{14}C]glucose, respectively. The synthesis of labeled OMP is accomplished through the sequential action of hexokinase, glucose-6-phosphate dehydrogenase, 6-phosphogluconate dehydrogenase, phosphoriboisomerase, 5-phosphoribosyl-1-pyrophosphate synthetase, and orotate phosphoribosyltransferase, as described previously (Rising et al., 1994), and is shown in Figure 1. The 1 mL reaction mixture contained 50 mM TEA, pH 7.8, 5 mM $MgCl_2$, 1 mM unlabeled glucose, 1 mM ATP, 0.15 mM $NADP^+$, 5 mM NH_4OAc, 2.5 mM orotate, 10 mM phosphoenolpyruvate, 10 mM $Mg(OAc)_2$, 10 mM α-ketoglutarate, and 50 μCi of [^{3}H]-glucose or 15 μCi of [^{14}C]glucose. Enzymes were added with hexokinase being added last to initiate the reaction. The progress of the reaction was determined by quantitating the product OMP on an HPLC DEAE column eluted with 10 mM sodium phosphate at pH 6 and monitored at 260 nm. The reaction was allowed to proceed for approximately 2 h, and OMP was purified on a MonoQ anion-exchange column eluted with a nonlinear 0−1 M NaCl gradient in 10 mM TEA buffer, pH 7.8. Fractions were analyzed for radioactivity using an LKB liquid scintillation counter. The overall yields, based on the conversion of radioactivity, were [1′-^{3}H]OMP, 30%; [4′-^{3}H]OMP, 86%; [5′-^{3}H]OMP, 78%; [1′-^{14}C]OMP, 34%; and [5′-^{14}C]OMP, 71%.

[2′-^{3}H]OMP was synthesized from [2′-^{3}H]ribose 5-phosphate (see Figure 1). The major impurity in [2′-^{3}H]ribose 5-phosphate was labeled ribulose 5-phosphate, which could be cleanly separated using MonoQ anion-exchange chromatography. The product OMP was purified as described above with a yield of *ca*. 50%. [1,3-$^{15}N_2$]OMP was prepared by replacing unlabeled orotate with [1,3-$^{15}N_2$]orotate. Approximately 15 μCi of [6-^{14}C]glucose was also added to the reaction mixture so the product [1,3-$^{15}N_2$,5′-^{14}C]OMP could be monitored by determining radioactivity. The product yield was approximately 70%.

Kinetic Isotope Effect Measurements. Labeled OMP, containing *ca*. 45 nCi of ^{3}H and *ca*. 11 nCi of ^{14}C in the appropriate positions, was mixed with unlabeled OMP to a final concentration of 200 μM. Five millimolar $MgCl_2$, 4 mM sodium pyrophosphate (PP_i), or 4 mM sodium phosphonoacetate (PA) and 100 mM Tris-HCl buffer at pH 8.0 were added to the reaction mixture. The mixture was divided into eight to ten, 250 μL portions, and either 1 μg of OPRTase, for reactions containing PP_i, or 50−100 μg of enzyme, for reactions containing PA, was added to start the reaction.

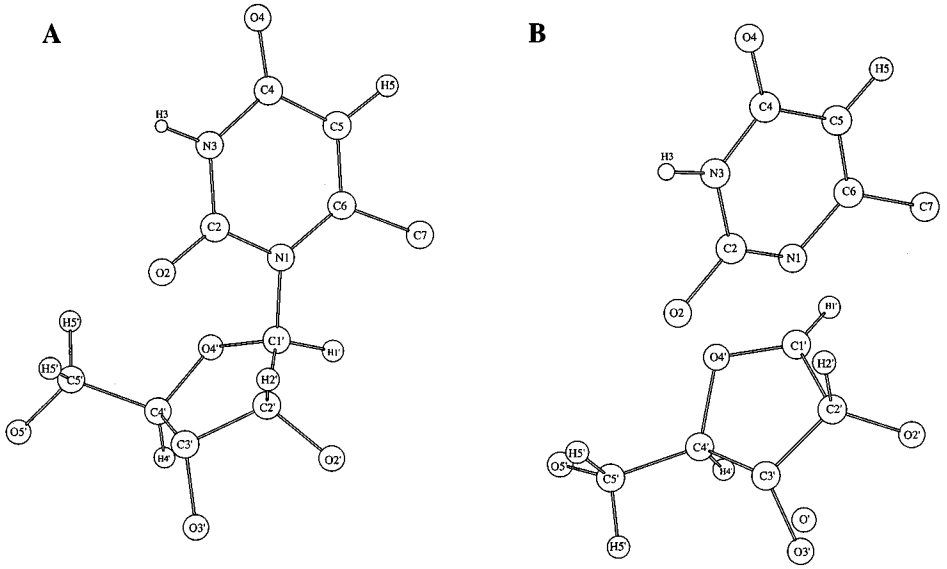

FIGURE 2: (A) Reactant state structure of OMP, minimized using MOPAC. (B) Transition state structure of OMP for the *S. typhimurium* OPRTase-catalyzed reaction. In both cases, the 5′-phosphate group and the two carboxyl oxygen atoms were excluded from the modeling and are omitted from the figure. The hydrogens of OH-2′, OH-3′, and CH-3′ were included in the modeling but are omitted from the figure for clarity. The critical bond lengths are listed in Table 1.

Samples were incubated at room temperature until a predetermined fractional conversion between $f = 20\%$ and $f = 75\%$ of OMP pyrophosphorolysis was achieved. The reaction was terminated by placing the sample into a boiling water bath for 2−3 min. One hundred microliter aliquots of each reaction mixture were injected onto a HPLC DEAE column for separation of OMP, and either PRPP or PRPA (5′-phosphoribosyl-1-phosphonoacetate), from the remaining OMP using elution with a linear 0−0.2 M NaCl gradient in 10 mM sodium phosphate, pH 6.0. The $^3H/^{14}C$ ratios, R_f, of the PRPP or PRPA product, and the unreacted OMP, were then determined by liquid scintillation counting. Radioactivity determinations were performed for 15 min and were repeated four to six times to obtain consistent $^3H/^{14}C$ ratios with standard errors less than 0.2%. For kinetic isotope effect calculations based on the remaining OMP substrate, the $^3H/^{14}C$ ratio at 0% conversion (R_0) was measured in the reaction mixture before the addition of OPRTase. For calculations based on product, $^3H/^{14}C$ dpm ratios (R_{100}) for PRPP were measured at a conversion of greater than 97%. The R_0 and R_{100} values in an individual experiment were within 1% of each other. For the reactions using phosphonoacetate as substrate, R_{100} was replaced by R_0 for the isotope effect calculations.

Tritium kinetic isotope effects ($^TV/K$) were measured by analyzing the $^3H/^{14}C$ ratio of unreacted [1′-^{3}H,5′-^{14}C]-, [2′-^{3}H,5′-^{14}C]-, [4′-^{3}H,5′-^{14}C], or [5′-^{3}H,5′-^{14}C]OMP, and of PRPP or PRPA formed from OMP, by using eqs 1 and 2, respectively (Tanaka et al., 1994).

$$^TV/K = 1.0 + \frac{\log R_f/R_0}{\log(1.0 - f)} \quad (1)$$

$$^TV/K = \frac{\log(1.0 - f)}{\log(1.0 - f(R_f/R_{100}))} \quad (2)$$

where f is the percent conversion of OMP to PRPP or PRPA, and it is calculated from the ratio of the dpm of the remaining [^{3}H]OMP to the starting [^{3}H]OMP in the reaction mixture.

Primary ^{14}C kinetic isotope effects and ^{15}N kinetic isotope effects were measured by analyzing the $^3H/^{14}C$ ratio of unreacted [1′-^{14}C,4′-^{3}H]- or [(1,3-^{15}N,5′-^{14}C),4′-^{3}H]OMP, and of PRPP or PRPA, by again using eqs 1 and 2, respectively, where $^TV/K$ is replaced by $^{14}V/K$ and where the reciprocals of the $^3H/^{14}C$ ratios were used as R_0, R_f, and R_{100} values. The measured $^{14}V/K$ kinetic isotope effects for unreacted substrate and product, multiplied by the respective $^TV/K$ values measured with [4′-^{3}H,5′-^{14}C]OMP provided kinetic isotope effects corrected for the remote tritium isotope effect at C-5′ (see below).

Computational Modeling. The modified BEBOVIB-IV program (Quantum Chemistry Program Exchange, No. 337, Sims et al., 1977) running on a Silicon Graphics Crimson was used to determine transition state structures for which the calculated kinetic isotope effect values match the measured kinetic isotope effect values. The bond lengths and angles in transition state structures were varied until calculated kinetic isotope effect values simultaneously satisfied all of the experimental results.

The initial reactant state structure of OMP was taken from the crystal structure of the OPRTase−OMP complex (Scapin et al., 1994), and standard values of C−H bond lengths were used. The structure was then optimized using AMPAC calculations at the precise level. For this modeling, a partial structure of OMP was used, with the 5′-phosphate group and two oxygen atoms of the orotate carboxylate group excluded from the calculations. The AMPAC-optimized reactant state structure is shown in Figure 2A.

The construction of transition state structures was based on previous studies on the hydrolysis of nucleosides (Horenstein et al., 1991). The starting structure for the transition state of the ribose ring used the crystal structure coordinates for ribonolactone (Kinoshita et al., 1981). The 5′-hydroxymethyl side chain was fixed at the reactant state conformation. The C−H bond lengths and angles of the ribose and orotate rings in the transition state were initially set equal to those of OMP. The C−H bond lengths, bond angles, and ring configurations were then optimized using

Table 1: Kinetic Isotope Effects for Reactions of OMP with PA by *S. typhimurium* OPRTase

substrates	isotope and type of effect	kinetic isotope effects	
		exptl	calcd
[1′-^{14}C]OMP + [4′-^{3}H]OMP	1′-^{14}C, primary	1.040 ± 0.004	1.042
[1′-^{3}H]OMP + [5′-^{14}C]OMP	1′-^{3}H, α-secondary	1.200 ± 0.007	1.201
[2′-^{3}H]OMP + [5′-^{14}C]OMP	2′-^{3}H, β-secondary	1.140 ± 0.007	1.141
[4′-^{3}H]OMP + [5′-^{14}C]OMP	4′-^{3}H, γ-secondary	0.988 ± 0.006	0.986
[5′-^{3}H]OMP + [5′-^{14}C]OMP	5′-^{3}H, δ-secondary	1.028 ± 0.008	1.028
[1,3-$^{15}N_2$,5′-^{14}C]OMP + [4′-^{3}H]OMP	1- ^{15}N, primary	1.006 ± 0.005	1.005

AM1 at the precise level. For the purpose of the modeling, an incoming oxygen nucleophile was modeled as an O′ atom with a molecular weight of phosphonoacetate (156 au), or alternatively as an O′ atom attached to a carbon atom of 140 au, and placed 180° opposite to the breaking C1′−N1 glycosidic bond. The degree of sp^2 hybridization at C1′, due to the formation of the oxocarbonium intermediate, can be described (Horentein et al., 1991; Parkin et al., 1991) as $\alpha = 90° + (19.5)$(C1′−N1 bond order), where α is the angle defined by C1′, N1, and any one of the three atoms attached to C1′.

Valence force constants for the various vibrational modes were obtained from reported values (Sims et al., 1974, 1984; Wilson et al., 1955), and the force constants for C−N modes were estimated from Badge's rule (Sims et al., 1984). The reaction coordinate was generated by coupling the stretching mode of C1′−N1 to that of C1′−O′ (Horenstein et al., 1991). The umbrella motion of the plane described by O4′−C1′−C2′ was incorporated into the reaction coordinate by introducing a weak coupling constant, 0.02, between the stretching modes of C1′−N1 and C1′−O′ and with the angular bending modes of C2′−C1′−N1, O4′−C1′−N1, C2′−C1′−O′, and H1′−C1′−O′ (Markham et al., 1987).

RESULTS AND DISCUSSION

Kinetic Isotope Effects. In determining kinetic isotope effects on enzyme-catalyzed reactions, a frequent concern is whether the observed kinetic isotope effects are intrinsic isotope effects (Cleland, 1982). In a number of cases, catalytic rates, k_{cat}, equivalent to or greater than the dissociation rates of the substrate from the enzyme−substrate complex (high "commitment" to catalysis; Cleland, 1982) result in observed isotope effects being lower than their intrinsic values. Numerous approaches to this problem have been used including conducting kinetic isotope effect measurements at pH values far away from the pH optimum such that catalysis is slowed and becomes the rate-determining step. A second method employs an alternative, "poor" substrate whose k_{cat} value is less than the normal substrate and whose steady-state K_m value is much higher.

For the pyrophosphorolysis of OMP to form PRPP and orotate, a value of 1.06 was observed at the pH optimum 7.8 for the α-secondary ^{3}H kinetic isotope effect. As the pH value decreases, the *V*/*K* value for OMP also decreases. At pH 4.7, we observed an increased value of 1.11 for the α-secondary kinetic isotope effect, but at both pH values, the primary ^{14}C kinetic isotope effect value remained unchanged (a value of less than 1.01 was determined). If the reaction occurs via an S_N2-like displacement at C1′, we would expect a value between 1.00 and 1.07 for the α-secondary ^{3}H kinetic isotope effect and almost no isotope effect for the primary ^{14}C kinetic isotope effect (Sinnott, 1990). The observed values are also inconsistent with a reaction mechanism involving a fully formed oxocarbonium transition state in a rate-limiting catalytic step. These results indicated that the observed kinetic isotope effect values are not fully expressed and that OMP retained a significant commitment even at low pH values.

We thus sought an analog of PP_i which would exhibit a decreased reaction rate and an increased steady-state K_m value, and phosphonoacetate (PA) appeared to be a good candidate. At pH 7.8, its V_{max} value is 0.11 unit/mg, which is 500 times less than that for PP_i, while its K_m is 1.86 mM, 40 times larger than that of PP_i. The overall 20 000-fold lower *V*/*K* value exhibited by PA suggests that any commitment exhibited by PP_i, which would attenuate the magnitude of kinetic isotope effects, would be diminished by using this substrate. Table 1 summarizes the kinetic isotope effects observed for the reaction of PA with OMP, catalyzed by *S. typhimurium* OPRTase. The kinetic isotope effect values are average values of 7−20 determinations of both the remaining substrate (OMP) and the product (PRPA) at different percentage conversions (25%−75%), and the uncertainties in the table are the standard deviations from these experiments. The values observed for the α-secondary ^{3}H and primary ^{14}C isotope effects were 1.20 and 1.04, respectively. A value of 1.14 was observed for the β-^{3}H isotope effect. The remote secondary isotope effects at H5′ and H4′ were also measured, and values of 1.028 for 5′-^{3}H and 0.988 for 4′-^{3}H were obtained.

Due to the availability of the doubly labeled [$^{15}N_{1,3}$]orotate, the measurement of the primary ^{15}N isotope effect was performed with OMP synthesized from this precursor. The observed ^{15}N isotope effect is close to unity (1.006). For an S_N1-like mechanism, a large primary ^{15}N isotope effect is predicted due to the essentially complete cleavage of the glycosidic bond (Horenstein el al., 1991), whereas for an S_N2-like mechanism, a smaller isotope effect is expected. The S_N2 mechanism seems unlikely, since all other isotope effects determined suggest an oxocarbonium ion transition state. The cleavage of the C1′−N1 bond in an S_N1-like mechanism gives rise to values of the primary ^{15}N isotope effect between 1.02 and 1.03 for related nucleoside hydrolysis reactions (Horenstein et al., 1991; Parkin et al., 1991). The small ^{15}N isotope effect obtained here suggests that the remote 3-^{15}N substitution may also contribute to the total observed ^{15}N isotope effect.

A previous study of isotope effects on the forward reaction (PRPP + orotate → OMP + PP_i) catalyzed by yeast OPRTase has been reported (Goitein et al., 1978). An α-secondary ^{3}H isotope effect of 1.17 and a primary ^{14}C isotope effect of 1.03 were measured using labeled PRPP. Considering the large uncertainties associated with those measurements, the values are in substantial agreement with

the values reported in this study. The theoretical maximum α-secondary ^{3}H kinetic isotope effect value calculated for S_N1-like transition states (the C1′−N1 bond is completely cleaved and a fully developed oxocarbonium is formed) is around 1.37. However, a more appropriate value for the intrinsic α-secondary ^{3}H kinetic isotope effect on glycosidic bond cleavage may be the values of 1.23−1.26 measured for the acid-catalyzed hydrolysis of AMP and inosine (Parkin et al., 1984). The value observed in the OPRTase-catalyzed reaction suggests that the transition state for this reaction proceeds with nearly complete formation of the oxocarbonium intermediate and with the C1′−N1 glycosidic bond substantially weakened.

The large β-secondary ^{3}H isotope effect observed in this study has precedence in the values reported for the enzyme-catalyzed hydrolysis of nucleosides (Schramm et al., 1991) and in the enzyme-catalyzed hydrolysis of glucosyl fluoride (Tanaka et al., 1994). These effects have been interpreted as a strong hyperconjugative interaction between H2′ and C1′, effectively ruling out an S_N2-type displacement at C1′. Isotopic substitution at the remote H5′ and H4′ positions should exhibit no isotope effect, unless the bonds associated with the heavy atoms are reorganized during the approach to the transtion state. The values reported in Table 1 for 5′-^{3}H and 4′-^{3}H isotope effects indicate that the conformation of the ribose ring and hydroxymethyl side chain are indeed perturbed in the transition state relative to free solution, giving rise to the significant isotope effects at H5′ and H4′ positions. Taken together, the magnitude of each of these kinetic isotope effects suggests that the use of phosphonoacetate as an alternative pyrophosphate analog allows the direct measurement of intrinsic kinetic isotope effects on the reaction. With this family of kinetic isotope effect values, the transition state structure was determined using the BEBOVIB method.

Transition State Modeling. The reactant state OMP structure, based on the reported crystal structure of the enzyme−OMP complex (Scapin et al., 1994), was further optimized using AM1 calculations and is shown in Figure 2A. This structure does not depict any interactions with side-chain residues from the enzyme, but in reality, significant interactions do exist from hydrogen bonding and van der Waals interactions (vide infra, Figure 3). The measured *V*/*K* kinetic isotope effects include isotope effects on steps from the binding of OMP through the transition state. In order to evaluate whether precatalytic enzyme−substrate interactions (e.g., binding isotope effects) would seriously compromise the calculation of kinetic isotope effect values, two hydrogen-bonding sites were selected: a hydrogen bond between N3 of the orotate ring and the main-chain carbonyl oxygen of Phe 35 and a hydrogen bond between orotate-O4 and the side-chain nitrogen of Arg 156. Trial calculations showed that the inclusion of these bonds led to recalculated values of the kinetic isotope effects that were within the experimental uncertainties of these measurements and could be ignored for the purposes of the transition state modeling.

The process of determining transition state structures was based on previous studies of the enzyme-catalyzed nucleoside hydrolysis (Schramm et al., 1994) and of the enzyme-catalyzed hydrolysis of glucosyl fluoride (Tanaka et al., 1994). To match calculated primary ^{14}C and α-secondary ^{3}H kinetic isotope effects, the bond lengths of C1′−H1′, C1′−O4′, C1′−C2′, and C1′−O′ (attacking nucleophile) were varied. It was assumed that C1′−C2′ and C1′−H1′ bond lengths at the transition state should be decreased from their reactant state lengths due to the sp^2 hybridization at C1′ and the hyperconjugative interaction of C2′−H2′ and C2′−N1. Therefore, during the iterative calculations, the C1′−C2′ and C1′−H1′ bond lengths were not allowed to exceed their bond lengths in the reactant state.

The β-secondary ^{3}H isotope effect at C2′ of 1.14 is near its maximum value and is believed to be largely the result of a strong hyperconjugative interaction with the neighboring C1′ atom. The kinetic isotope effect value is maximal when the dihedral angle between C2′−H2′ and C1′−N1 is nearly eclipsed (Sunko et al., 1977). At this dihedral angle, the calculated KIE value is only sensitive to C2′−H2′ bond length changes, and shortening C2′−H2′ by 4.5% produces a calculated value which matches the experimentally determined value.

The remote 5′-^{3}H and 4′-^{3}H kinetic isotope effects were modeled independently of changes at C1′, C2′, O4′, or the orotate ring, and changes in the C4′−H4′ and C5′−H5′ bond lengths or angles had no effect on other calculated isotope effects. A small change in the C4′−H4′ bond length (lengthened by 9%) was sufficient to obtain a fit between the calculated and measured 4′-^{3}H kinetic isotope effect values. For the 5′-^{3}H kinetic isotope effect, changes in the C4′−C5′−H5′ angle alone were insufficient to yield a reasonable match, and a small increase in the C5′−H5′ bond length of 8% was required to obtain a match between the observed and calculated kinetic isotope effect.

Perhaps the most unexpected result from this study is the small magnitude of the ^{15}N effect. Since this value is the combination of isotope effects at both the N1 and N3 positions, variations in both N1 and N3 bond orders were performed in order to match the experimental isotope effect. In the transition state, the departing orotate ring develops a partial negative charge, and resonance interactions allow this charge to be delocalized to the O4 oxygen atom, which forms a strong hydrogen-bonding interaction with the guanidino nitrogens of Arg 156 and the backbone NH of Phe 34 of the enzyme. However, calculations show that resonance delocalization of the C1′−N1 bond to generate the C4 enolate still results in a calculated ^{15}N kinetic isotope effect of 1.02, significantly larger than the observed effect. Additional variation in bonding at N3 is similarly insufficient to match the measured kinetic isotope effect value. An alternate resonance delocalization involves the formation of the enolate anion at the C2 keto group of the orotate ring, with the negative charge on the C2 oxygen atom potentially stabilizing the developing positive charge in the ribose ring. Variations of N1−C2 and C2−O2 bond lengths, together with the changes in the polarizibilities of N3−H3 and C4−O4 (formation of partial positive and negative charges on H3 and O4, respectively), yielded a calculated value which matched the measured value.

Table 1 tabulates the experimental kinetic isotope effects together with those calculated for the structural model described here. Reasonable agreement is shown for all the isotope effects. Some critical bond lengths for both the reactant state and the transition state structures are presented in Table 2. The uncertainties in Table 2 reflect the statistical errors observed in the measurements. Figure 2B illustrates the transition state structure modeled here, with the omission of hydroxyl H atoms, the C5′−phosphate group, and the

Table 2: Key Bond Lengths for the Reactant State (RS) and the Transition State (TS) of OMP in the Reaction Catalyzed by *S. typhimurium* OPRTase

bond	length (Å) (RS)[a]	length (Å) (TS)[b]	bond	length (Å) (RS)[a]	length (Å) (TS)[b]
C1′−N1	1.465	1.85 ± 0.05	N1−C2	1.420	1.30 ± 0.04
C1′−O4′	1.435	1.31 ± 0.02	C2−O7	1.254	1.38 ± 0.05
C1′−C2′	1.563	1.54 ± 0.01	N3−C4	1.406	1.35 ± 0.04
C1′−H1′	1.136	1.133 ± 0.001	N3−H8	0.994	1.180 ± 0.002
C2′−H2′	1.122	1.171 ± 0.001	C4−O9	1.252	1.30 ± 0.04
C4′−H4′	1.124	1.135 ± 0.001	C1′−O′		3.8 ± 0.3
C5′−H5′	1.127	1.137 ± 0.001			

[a] Bond lengths are initially obtained from the OMP crystal structure and from AM1 calculations. [b] Bond lengths are derived from the BEBOVIB calculation, and uncertainties reflect the experimental errors.

carboxylate oxygen groups in the orotate ring. In the transition state structure, the C1′−N1 bond length is 1.85 Å (compared to 1.46 Å in the reactant state), corresponding to a bond order of 0.28. This bond breaking is also accompanied by a partial double bond formation at C1′−O4′. The C1′−O′ distance of 3.8 Å reflects the essential absence of bonding between C1′ and the attacking nucleophile. In the orotate ring, the shorter N1−C2 bond length and the longer C2−O2 bond length show the predominant resonance delocalization of the C1′−N1 bond toward the C2 orotate oxygen.

The large β-secondary ^{3}H isotope effect determined in this study suggests that, in the transition state, the ribose ring adopts a conformation with a dihedral angle between H2′−C2′ and C1′−N1 at or near 0°. This conformation maximizes the overlap between the occupied σ-orbital of C2′−H2′ bond and the p-orbital of C1′, resulting in the maximum hyperconjugative interaction and stabilization of the oxocarbonium ion developed in the transition state. A potential hydrogen bond between the 2′-hydroxyl group and the orotate carboxyl oxygen atoms may further stabilize the oxocarbonium ion through inductive effects (Johnson et al., 1988). This would also result in the shortening of the C2′−H2′ bond length, as found in this study. The small, inverse 4′-^{3}H kinetic isotope effect and the large, normal 5′-^{3}H kinetic isotope effect are consistent with other studies in which an oxocarbonium ion is formed in the transition state (Horenstein et al., 1991; Tanaka et al., 1994). The crystal structures of the E−OMP (Scapin et al., 1994) and E−PRPP−orotate complexes (Scapin et al., 1995) indicate that the 5′-phosphate group is restrained in the Thr 128−Thr 131 loop during the reaction, due to multiple hydrogen-bonding interactions (see Figure 3). Thus, the 5′-hydroxymethyl group retains a reactant state conformation in the transition state, potentially resulting in the distortion of the C4′−C5′−O5′ angle during the change of the ribose ring conformation accompanying oxocarbonium ion formation. Its is likely that this distortion results in the observed remote isotope effects. Lengthening of the C4′−H4′ bond length and a change in bond angles and bond lengths involving the two H5′ atoms have permitted us to match the calculated kinetic isotope effect values to the observed ones.

Chemical Mechanism. The partial C1′−N1 bond cleavage and double bond formation in C1′−O4′ argue that the reaction undergoes an S_N1-like mechanism, with a substantially developed oxocarbonium ion in the transition state. The oxocarbonium ion is reactive and unstable, and it needs to be stabilized in the enzyme active site. In the case of

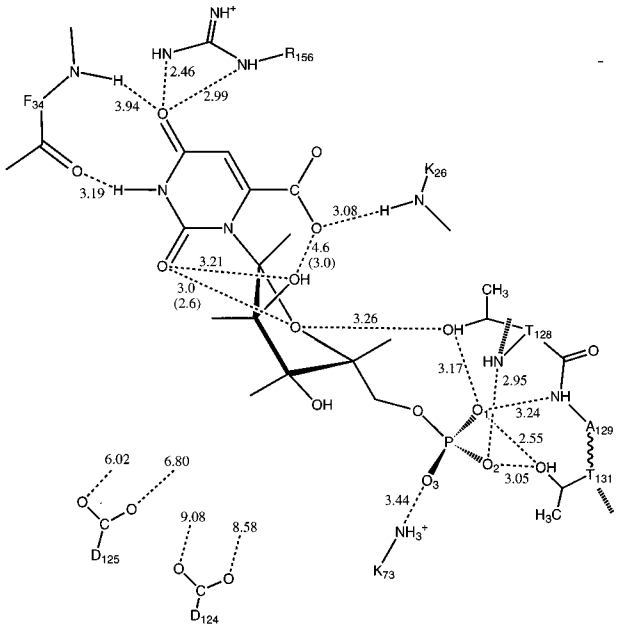

FIGURE 3: Hydrogen-bonding interactions between OPRTase and OMP. The coordinates are from Scapin et al. (1994).

glycosidase catalysis, carboxylate residues in the active site of the enzyme interact with the positively charged transition state entity to stabilize the oxocarbonium (Tanaka et al., 1994; Sinnott et al., 1990; Kajimoto et al., 1991). In the case of *S. typhimurium* OPRTase, it is clear from the crystal structures of the E−OMP and E−PRPP−orotate complexes that this function could be fulfilled by the paired Asp 125 and Asp 124 residues, which are highly conserved in PRTases and PRPP synthetase. However, these residues are *ca.* 6 and *ca.* 8.6 Å, respectively, from C1′ of OMP. It is also clear from comparisons of the E−OMP and E−PRPP−orotate complexes (Figure 4) that the anomeric carbon of the ribosyl 5′-phosphate cation swings through a 7 Å arc from its position in the E−OMP complex to its position in the E−PRPP−orotate complex. The ribosyl 5′-phosphate cation is firmly tethered by the numerous hydrogen-bonding interactions with the Thr 128−Thr 131 loop (Figure 3) and must additionally twist to generate the observed α configuration at C1 in PRPP. Together with our transition state information, we can propose a reasonably detailed chronology of catalysis occurring on the surface of OPRTase.

Although the kinetic mechanism is random (Bhatia et al., 1990), the tighter binding of OMP (K_m = 3 μM) versus inorganic pyrophosphate (K_m = 30 μM) suggests that the E−OMP complex will form preferentially. The interaction of Lys 73 with the 5′-phosphate is disrupted by pyrophosphate binding, and this could represent the interaction which reorganizes ground state enzyme−substrate interactions and initiates catalysis, thus preventing nonproductive hydrolysis via solvent capture of the oxocarbonium ion. This loss of the 5′-phosphate−Lys 73 interaction also may allow for the interaction between the 5′-phosphate and phosphate binding loop interactions to become stronger and initiate the movement of the ribose 5′-phosphate ring away from the orotate ring. The O4′ ring oxygen initiates oxocarbonium ion formation by electron donation into the C1′−O4′ bond, with subsequent lengthening of the C1′−N1 bond. Rehydridization of the C1′ center brings both O4′ and the 2′-hydroxyl closer to the C2 keto oxygen of the orotate ring, accommodating the increased electron density from the C1′−N1

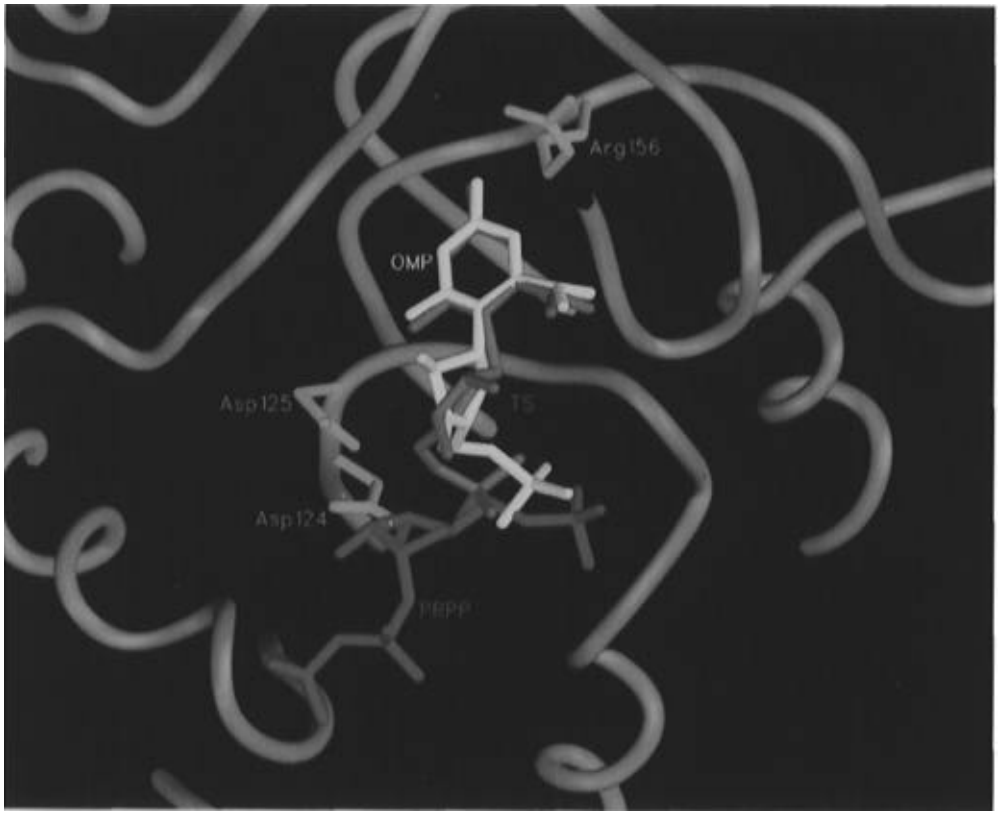

FIGURE 4: Structures of the binary OPRTase−OMP, OPRTase−PRPP, and hypothetical OPRTase−transition state complexes. The coordinates are from Scapin et al. (1994) (OPRTase−OMP) and Scapin et al. (1995) (OPRTase−PRPP).

bond to be stabilized at this position. The lengthening of the C1′−N1 bond also enhances the interaction of the C4 keto and N3 amido groups with the backbone atoms of Phe 34, shortening and further polarizing these hydrogen bonds. In the transition state, the C1′−N1 bond has increased from 1.46 to 1.85 Å, while the C1′−O4′ bond has shortened from 1.43 to 1.31 Å. Both orotate keto oxygen bond lengths have lengthened, dispersing the buildup of negative chage on the orotate ring. Strong hydrogen bonds have been formed between the 2′-OH and both C2 keto oxygen and orotate carboxyl groups. This accounts for the much poorer substrate activity observed for orotate methy ester (Bhatia et al., 1993). Overall, this bipolar transition state, with the orotate ring building up negative charge and the ribose ring building up positive charge, is energetically stabilized via both "intramolecular" and enzyme−transition state interactions.

To prevent the collapse of the transition state back to starting materials, the C1′−N1 bond must be further lengthened, and compensating stabilization of charges must occur. In the orotate ring, this is likely to be accomplished by drawing the charge out of the C2 keto group and into the C4 keto group by further shortening of the Phe 34, C4 keto oxygen distance (*ca.* 3.2 Å in the E−orotate complex). As the intramolecular stabilization decreases, and as the 5′-phosphate is pulled further into the phosphate binding loop, the swinging movement of the ribosyl 5′-phosphate cation is likely initiated by the long-range electrostatic attraction between the oxocarbonium ion and Asp 125. There are only hydrophobic residues located in the base of the channel which connects the orotate and PP_i binding sites, allowing for the unencumbered movement for the tethered ribosyl 5′-phosphate cation. The approach of the *re* face of the oxocarbonium ion to bound PP_i results in the formation of the covalent C1−O−PP_i bond in the α-anomeric configuration.

The model of catalysis presented here satisfies many of the observations made in this and other studies of the chemical mechanism of OPRTase. Several key questions remain to be answered. First, the essential role of Mg^{2+} in catalysis, not addressed here, may be to either assist in the binding of PP_i (Bhatia et al., 1993) or additionally influence chemical steps. Second, the suspected critical nature of the conserved dicarboxylate motif (Asp 124 and Asp 125 in OPRTase) remains to be fully delineated, although one possible function may the initiation of ribosyl phosphate cation translation toward the bound PP_i and stabilization of the transtion state, as proposed here. Finally, the translation of the ribosyl phosphate cation must occur in an environment from which solvent is rigorously excluded to prevent the rapid reaction of solvent with this reactive intermediate. A mobile surface loop which contains conserved lysine residues (K100 and K103; Ozturk et al., 1995) which are important for catalysis is present in OPRTase, but the temporal and spatial coupling between loop movement and catalysis is unclear at this time. Nevertheless, we believe that the details of catalysis by OPRTase described here will guide future experiments aimed at answering these remaining questions.

ACKNOWLEDGMENT

We thank Dr. D. Ozturk for the generous supplies of enzyme used in this study and Dr. G. Scapin for assisting in the preparation of Figure 4.

REFERENCES

Bhatia, M. B., & Grubmeyer, C. (1993) *Arch. Biochem. Biophys. 303,* 321.

Bhatia, M. B., Vinitsky, A., & Grubmeyer, C. (1990) *Biochemistry 29*, 10480.
Chelsky, D., & Parsons, S. (1975) *J. Biol. Chem. 250*, 5669.
Cleland, W. W. (1982) *CRC Crit Rev. Biochem. 13*, 385.
Frisch, M. J., Truchks, G. W., Hend-Gordon, M., Gill, P. M. W., Wong, M. W., Foresman, J. B., Johnson, B. G., Schlegel, H. B., Robb, M. A., Replogle, E. S., Gomperts, R., Andres, J. L., Raghavachari, K., Binkley, J. S., Gonzalez, C., Stewart, J. J. P., & Pople, J. A. (1992) *Gaussian 92 User's Guide*, Gaussian Inc., Pittsburgh, PA.
Goitein, R. K., Chelsky, D., & Parsons, S. M. (1977) *J. Biol. Chem. 253*, 2963.
Hersey, L. T., & Taylor, M. (1986) *Gene 93*, 287.
Horenstein, B. A., & Schramm, V. L. (1993) *Biochemistry 32*, 9917.
Horenstein, B. A., Parkin, D. W., Estupinan, B., & Schramm, V. L. (1991) *Biochemistry 30*, 10788.
Hove-Jensen, B., Harloro, K. W., King, C. J., & Switzer, R. L. (1986) *J. Biol. Chem. 261*, 6765.
Johnson, R. W., Marschner, T. M., & Oppenheimer, N. J. (1988) *J. Am. Chem. Soc. 110*, 2257.
Kajimoto, T., Liu, K. K.-C., Pederson, R. L., Zhong, Z., Ichikawa, Y., Porco, J. A., & Wong, C.-H. (1991) *J. Am. Chem. Soc. 113*, 6187.
Kinoshita, Y., Ruble, J. R., & Jeffrey, G. A. (1981) *Carbohydr. Res. 92*, 1.
Kirby, A. J. (1987) *CRC Crit. Rev. Biochem. 22*, 283.
Kline, P. C., & Schramm, V. L. (1993) *Biochemistry 32*, 13212.
Markham, G. C., Parkin, D. W., Mentch, F., & Schramm, V. L. (1987) *J. Biol. Chem. 262*, 5609.
Mentch, F., Parkin, D. W., & Schramm, V. L. (1987) *Biochemistry 26*, 921.
Merkler, D. J., Kline, P. C., Weiss, P., & Schramm, V. L. (1993) *Biochemistry 32*, 12993.
Musick, D. L. (1981) *CRC Crit. Rev. Biochem. 11*, 1.
Ozturk, D. H., Dorfman, R. H., Scapin, G., Sacchettini, J. C., & Grubmeyer, C. (1995) *Biochemistry 34*, 10755.
Parkin, D. W., Leung, H. B., & Schramm, V. L. (1984) *J. Biol. Chem. 259*, 9411.
Parkin, D. W., Mentch, F., Banks, G. A., Horenstein, B. A., & Schramm, V. L. (1991) *Biochemistry 30*, 4586.
Rising, K. A., & Schramm, V. L. (1994) *J. Am. Chem. Soc. 116*, 6531.
Scapin, G., Sacchettini, J. C., Dessen, A., Bhatia, M. B., & Grubmeyer, C. (1993) *J. Mol. Biol. 230*, 1304.
Scapin, G., Grubmeyer, C., & Sacchettini, J. C. (1994) *Biochemistry 33*, 1287.
Scapin, G., Ozturk, D. H., Grubmeyer, C., & Sacchettini, J. C. (1995) *Biochemistry 34*, 10744.
Schramm, V. L., Horenstein, B. A., & Kline, P. C. (1994) *J. Biol. Chem. 269*, 18259.
Sims, L. B., & Fry, A. (1974) *Special Publication No. 1*, University of Arkansas, Fayetteville, AR.
Sims, L. B., & Lewis, D. E. (1984) *Isot. Org. Chem. 6*, 161.
Sims, L. B., Burton, G. W., & Lewis, D. E. (1977) *Quantum Chemistry Program Exchange, No. 337*, Indiana University, Bloomington, IN.
Sinnott, M. L. (1990) *Chem. Rev. 90*, 1171.
Stout, J. T., & Caskey, C. T. (1989) in *The Metabolic Basis of Inherited Disease* (Scriver, C. R., Beaudet, L., Sly, W. S., & Valle, D., Eds.) pp 1007−1028, McGraw-Hill, New York.
Sunko, D. E., Szele, I., & Hehre, W. J. (1977) *J. Am. Chem. Soc. 99*, 5000.
Tanaka, Y., Tao, W., Blanchard, J. S., & Hehre, E. J. (1994) *J. Biol. Chem. 269*, 32306.
Victor, J., Greenderg, L. B., & Sloan, D. L. (1979) *J. Biol. Chem. 254*, 2647.
Wilson, E. B., Desius, J. C., & Cross, P. C. (1955) *Molecular Vibrations*, McGraw-Hill Co., Inc., New York.

BI951898L